Monthly Notices
of the
ROYAL ASTRONOMICAL SOCIETY

Mon. Not. R. Astron. Soc. **424,** 1297–1306 (2012) doi:10.1111/j.1365-2966.2012.21311.x

Multiwavelength observations of the Type IIb supernova 2009mg⋆

S. R. Oates,[1]† A. J. Bayless,[2] M. D. Stritzinger,[3,4,5] T. Prichard,[2,6] J. L. Prieto,[7]‡ S. Immler,[8,9,10] P. J. Brown,[11] A. A. Breeveld,[1] M. De Pasquale,[12] N. P. M. Kuin,[1] M. Hamuy,[13] S. T. Holland,[14] F. Taddia[4] and P. W. A. Roming[2,6]

[1]*Mullard Space Science Laboratory, University College London, Holmbury St. Mary, Dorking, Surrey RH5 6NT*
[2]*Space Science and Engineering, Division 15, Southwest Research Institute, Building 263, 6220 Culebra Road, San Antonio, TX 78238, USA*
[3]*Department of Physics and Astronomy, Aarhus University, Ny Munkegade 120, DK-8000 Aarhus C, Denmark*
[4]*Department of Astronomy, The Oskar Klein Centre, Department of Astronomy, Stockholm University, AlbaNova, 10691 Stockholm, Sweden*
[5]*Carnegie Observatories, Las Campanas Observatory, La Serena, Chile*
[6]*Department of Astronomy and Astrophysics, Pennsylvania State University, 104 Davey Laboratory, University Park, PA 16802, USA*
[7]*Department of Astrophysical Sciences, Princeton University, Peyton Hall, Princeton, NJ 08544, USA*
[8]*Department of Astronomy, University of Maryland, College Park, MD 20742, USA*
[9]*Astrophysics Science Division, Code 660.1, NASA Goddard Space Flight Centre, 8800 Greenbelt Road, Greenbelt, MD 20771, USA*
[10]*Centre for Research and Exploration in Space Science and Technology Code 668.8 8800, Greenbelt Road Goddard Space Flight Centre, Greenbelt, MD 20771, USA*
[11]*Department of Physics & Astronomy, University of Utah, 115 South 1400 East #201, Salt Lake City, UT 84112, USA*
[12]*Department of Physics and Astronomy, University of Nevada, Las Vegas 4505 S. Maryland Parkway, Las Vegas, NV 89154, USA*
[13]*Departamento de Astronomía, Universidad de Chile, Santiago, Chile*
[14]*Space Telescope Science Institute, 3700 San Martin Drive, Baltimore, MD 21218, USA*

Accepted 2012 May 15. Received 2012 May 1; in original form 2012 February 17

ABSTRACT

We present *Swift* Ultra-Violet Optical Telescope and X-Ray Telescope (XRT) observations, and visual wavelength spectroscopy of the Type IIb supernova (SN) 2009mg, discovered in the Sb galaxy ESO 121-G26. The observational properties of SN 2009mg are compared to the prototype Type IIb SNe 1993J and 2008ax, with which we find many similarities. However, minor differences are discernible including SN 2009mg not exhibiting an initial fast decline or *u*-band upturn as observed in the comparison objects, and its rise to maximum is somewhat slower leading to slightly broader light curves. The late-time temporal index of SN 2009mg, determined from 40 d post-explosion, is consistent with the decay rate of SN 1993J, but inconsistent with the decay of ^{56}Co. This suggests leakage of γ-rays out of the ejecta and a stellar mass on the small side of the mass distribution. Our XRT non-detection provides an upper limit on the mass-loss rate of the progenitor of $\dot{M} < 1.5 \times 10^{-5}$ M$_\odot$ yr^{-1}. Modelling of the SN light curve indicates a kinetic energy of $0.15^{+0.02}_{-0.13} \times 10^{51}$ erg, an ejecta mass of $0.56^{+0.10}_{-0.26}$ M$_\odot$ and a ^{56}Ni mass of 0.10 ± 0.01 M$_\odot$.

Key words: supernovae: individual: SN 2009mg.

1 INTRODUCTION

Core collapse supernovae (SNe) are the death throws of massive stars. These stellar explosions are classified into Type II and Type Ib/c subtypes depending on their spectroscopic characteristics. The spectra of Type II SNe (SNe II) contain prevalent hydrogen lines, while those of SNe Ib lack hydrogen lines, but display lines of helium. The spectra of SNe Ic, on the other hand, lack both hydrogen and helium lines (see Filippenko 1997, for further details and references). The lack of hydrogen lines in SNe Ib/c is thought to be due to the hydrogen envelope being stripped before the final pre-SNe stage is reached. In the case of SNe Ic, the helium envelope is also thought to be stripped or ^{56}Ni is not sufficiently mixed into any helium layer and thereby prevents the excitation of helium lines. The progenitors of SNe Ib/c are therefore thought to be stars in which the majority of their hydrogen-rich envelope is stripped via stellar winds and/or transferred to a secondary star via Roche

⋆ This paper includes data gathered with the 6.5-m Magellan telescopes located at Las Campanas Observatory, Chile, and the Gemini Observatory, Cerro Pachon, Chile (Gemini Programmes GS-2009B-Q-9, GS-2009B-Q-40 and GS-2009B-Q-67).

†E-mail: sro@mssl.ucl.ac.uk
‡Hubble, Carnegie-Princeton Fellow.

lobe overflow (e.g. Wheeler & Levreault 1985; Woosley, Langer & Weaver 1993, 1995).

In 1987, hints appeared of a new subclass of SNe II from the spectral evolution of the peculiar SN 1987K (Filippenko 1988). Around maximum light SN 1987K exhibited spectral characteristics reminiscent of a normal SN II event including the presence of a broad Hα absorption feature. However, nearly five months later, when the object reappeared from behind the sun, its spectrum resembled more closer that of an SN Ib. This peculiar spectral metamorphosis provided a hint that normal SNe II maybe linked to the hydrogen-stripped SN Ib subclass. Similarly, the well-observed SN 1993J exhibited a clear SN II-like spectrum just after explosion, but over several weeks its spectrum evolved to resemble that of a classic SN Ib event with dominant He I features (Filippenko, Matheson & Ho 1993; Swartz et al. 1993). This led to the introduction of the Type IIb subclass (Filippenko 1988). SNe IIb progenitors are able to retain a small amount ($\sim$0.01 $M_\odot$) of hydrogen at the time of explosion, and this residual hydrogen shell is manifested in the optical spectrum obtained just after explosion (Nomoto et al. 1993; Podsiadlowski et al. 1993). Recently, it has been proposed that SNe IIb may be further classified into Type eIIb and cIIb subclasses, dividing SNe IIb into extended or compact progenitors, respectively (Chevalier & Soderberg 2010). This subclassification depends on the radius and mass-loss history of the progenitor star, which may be determined from X-ray and radio observations. Examples of SNe eIIb are SN1993J and 2001dg, while examples of SNe cIIb are 1996cb, 2001ig and 2008ax (Chevalier & Soderberg 2010).

Over the past 20 years, approximately 72[1] (Barbon et al. 1999) SNe IIb have been discovered, but only a handful have been well observed including, amongst others, SNe 1987K (Filippenko 1988), 1993J (Schmidt et al. 1993), 1996cb (Qiu et al. 1999), 2003bg (Hamuy et al. 2009), 2008ax (Pastorello et al. 2008; Roming et al. 2009a; Chornock et al. 2011; Taubenberger et al. 2011) and most recently 2011dh (Arcavi et al. 2011; Maund et al. 2011; Soderberg et al. 2012). The exact number of SNe IIb is uncertain due to the evolution of their spectra. If spectral observations of SNe IIb are not obtained early enough, then we may miss SNe II-like features, such as prevalent hydrogen lines, and so misidentify SNe IIb as SNe Ib. Conversely, if late-time spectral observations are not obtained or are too poor for line identification, then the development of SN Ib-like features, such as numerous He I lines, may not be detected and so the SN could be misidentified as an SN II. Currently, little is known about the spread in mass and energy of SNe IIb, the exact manner of mass-loss, nor exactly how they relate SNe II and SNe Ib/c. It is important that an expanded sample of well-observed SNe IIb is constructed as these objects with their small hydrogen envelope may bridge the gap between normal SNe II and SNe Ib/c.

Direct information can be gathered on the progenitors of SN from pre-explosion images, but it is difficult to identify candidate progenitors without high-resolution *Hubble Space Telescope* images. Candidate progenitor stars have been directly detected in pre-explosion images of the Type IIb SNe 1993J and 2011dh. In the case of SN 1993J, a K-type supergiant in a binary system was determined to be its progenitor (Maund et al. 2004). For SN 2011dh, a mid-F-type yellow supergiant is observed at the location of the SN (Maund et al. 2011; Van Dyk et al. 2011), but it is currently too soon to determine whether this is the star that exploded, the binary companion, or an unrelated star (Arcavi et al. 2011; Bietenholz et al. 2012; Soderberg et al. 2012). Evidently, further observations are required after SN 2011dh has faded to determine if the candidate star has disappeared or is indeed still present.

[1] http://heasarc.gsfc.nasa.gov/W3Browse/star-catalog/asiagosn.html

1.1 Supernova 2009mg

In this paper, we present broad-band ultraviolet (UV) and optical light curves and visual-wavelength spectroscopy of the Type IIb SN 2009mg. SN 2009mg was discovered on the 7.9 December 2009 UT (Monard 2009) in the Sb galaxy ESO 121-G26. With J2000 coordinates of RA $= 6^{\rm h}\,21^{\rm m}\,44\overset{\rm s}{.}86$ Dec. $= -59^\circ\,44'\,26''$, SN 2009mg was 46 arcsec east and 4 arcsec south from the centre of the host galaxy. The redshift of the host galaxy is $z = 0.0076 \pm 0.0001$ (Koribalski et al. 2004). The distance to the host galaxy is therefore 32.7 Mpc and the distance modulus is $\mu = 33.01 \pm 0.48$ mag, both of which were retrieved from the NASA/IPAC Extragalactic Database.[2]

As commonly found for SNe IIb, the classification was continually revised as the object evolved. The initial classification was that of an SN Ia (Prieto 2009); however, soon after this it was changed to a broad-line SN Ic (Roming, Prieto & Milne 2009b). Days later as the spectrum evolved, it was clear that this object was an SN IIb (Stritzinger 2010), as its early spectra strongly resembled that of the prototypical Type IIb SNe 1993J and 1996cb. SN 2009mg was not the first SN to be detected in ESO 121-G26. In the previous year, the Type II SN 2008M was also discovered in this galaxy (Green 2008). The locations of both SNe 2009mg and 2008M are indicated in Fig. 1.

The organization of this paper is as follows. In Section 2, we provide the main observations of this SN, and describe the data reduction and analysis methods used. The main results are presented in Section 3, while the discussion and conclusions follow in Section 4 and Section 5, respectively. Unless stated, all uncertainties throughout this paper are quoted at 1σ. We have adopted the Hubble parameter $H_0 = 70\,{\rm km\,s^{-1}\,Mpc^{-1}}$ and density parameters $\Omega_\Lambda = 0.73$ and $\Omega_{\rm m} = 0.27$.

2 OBSERVATIONS

2.1 *Swift* imaging

X-ray and optical/UV observations were performed simultaneously with the X-Ray Telescope (XRT; Burrows et al. 2005) and the Ultra-Violet Optical Telescope (UVOT; Roming et al. 2000, 2004, 2005), the two narrow-field instruments onboard *Swift* (Gehrels et al. 2004). The analysis of 57.5 ks of X-ray data, see Fig. 2, does not reveal a source at the position of the SN. In Section 3.4, the XRT observations are used to place limits on the mass-loss rate of the progenitor.

Optical/UV observations of both SNe 2008M and 2009mg were obtained with *Swift*. SN 2008M was observed over seven epochs from 28.9 January 2008 UT until 5.3 February 2008 UT. These images were obtained from the *Swift* archive and used to construct deep template images, which were then used to subtract away galaxy

[2] http://ned.ipac.caltech.edu/ The NASA/IPAC Extragalactic Database (NED) is operated by the Jet Propulsion Laboratory, California Institute of Technology, under contract with the National Aeronautics and Space Administration.

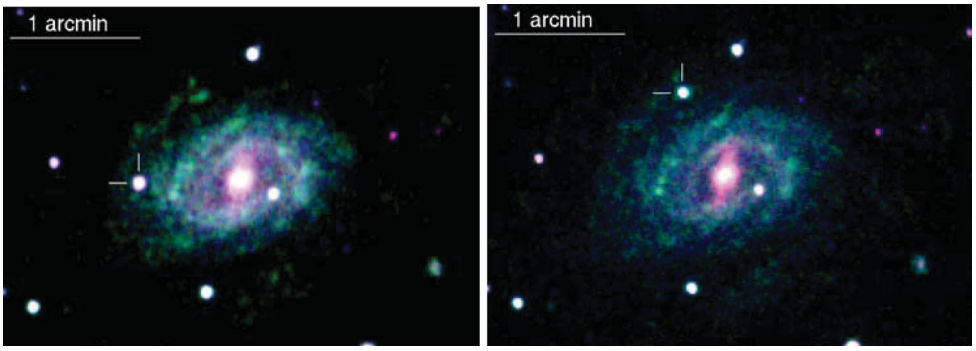

Figure 1. Two panels displaying the *Swift* UVOT images of the galaxy ESO 121-G26 and SNe 2009mg (left) and 2008M (right), respectively. The RGB images were constructed from *u*, *b* and *v* images.

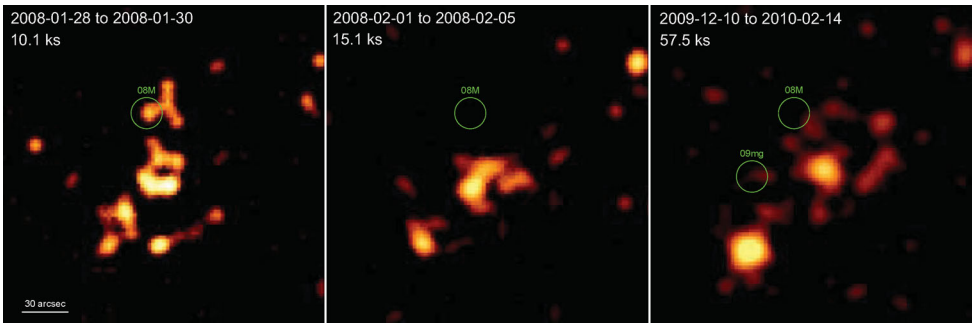

Figure 2. The three panels display the *Swift* XRT images of the galaxy ESO 121-G26 at three different epochs. The first panel consists of data from a 2 d period displaying the X-ray emission from SN 2008M. The middle panel consists of data from a 4 d period, and shows that the X-ray emission from SN 2008M has faded. The final panel shows the position of SN 2008M and SN 2009mg. No X-ray emission is detected from SN 2009mg.

emission at the position of SN 2009mg in each of the science images.

Swift UVOT observations of SN 2009mg commenced on 10.9 December 2009 UT and concluded on 14.4 February 2010 UT. 22 epochs of broad-band imaging was performed using three optical (*u*, *b* and *v*) and three UV (*uvw*1, *uvm*2 and *uvw*2) filters.

Photometry of SN 2009mg was computed following the method described in Brown et al. (2009). The SN+galaxy photometry was extracted using a 3 arcsec radius source region and a background region positioned away from the galaxy in a source-free location. The galaxy count rate was determined from the summed exposures of SN 2008M, using the same background and source regions. This value was then subtracted from the SN+galaxy photometry determined from the images of SN 2009mg. The SN photometry was then aperture corrected to 5 arcsec in order to be compatible with UVOT calibration. The analysis pipeline used software HEADAS 6.10 and UVOT calibration 20111031. Count rates were converted into magnitudes using the UVOT zero-points presented by Breeveld et al. (2011). The resulting light curves are presented in Fig. 3 and the photometry is provided in Table 1. For some of the UV data points, several epochs have been co-added to provide detections or deep upper limits.

2.2 Optical spectroscopy

Nine epochs of low-resolution and one epoch of high-resolution optical spectroscopy were obtained with facilities located at the Las Campanas Observatory and the Gemini-South (GEMINI-S) telescope. A journal of the spectroscopic observations is provided in Table 2. Our spectroscopic series covers the flux evolution from −1.2 to +91.6 d relative to *B*-band maximum. All spectra were reduced in the standard manner using IRAF scripts,[3] and in most cases, telluric corrections were not performed.

3 ANALYSIS

3.1 Reddening

According to the Schlegel, Finkbeiner & Davis (1998) infrared (IR) dust maps, the Galactic reddening component in the direction of SN 2009mg is $E(B-V)_{\rm MW} = 0.045$ mag. In order to estimate the colour excess attributed to dust in the host galaxy of SN 2009mg, we turn to two methods.

First, from close examination of our high-resolution MIKE spectrum obtained on 24.2 December 2009 UT (551 89.24 MJD) we identify Na I D1 λ5931.9 and Na I D2 λ5937.9, shown in Fig. 4, at the redshift of the host galaxy. From this, we measure an equivalent width (EW) for Na I D1 of 0.21 Å. Following the Munari & Zwitter (1997) relation between $E(B-V)$ and EW of Na I D1 implies a host galaxy colour excess of $E(B-V)_{\rm host} = 0.07 \pm 0.02$ mag.

We have also estimated the host galaxy colour excess by determining the offset of the $b-v$ colour curve of SN 2009mg with respect to a template colour curve (Drout et al. 2011; Stritzinger et al., in preparation). This template colour curve was constructed from a sample of six unreddened SNe Ib/c and SNe IIb, which were

[3] IRAF is distributed by the National Optical Astronomy Observatories, which are operated by the Association of Universities for Research in Astronomy, Inc., under cooperative agreement with the National Science Foundation.

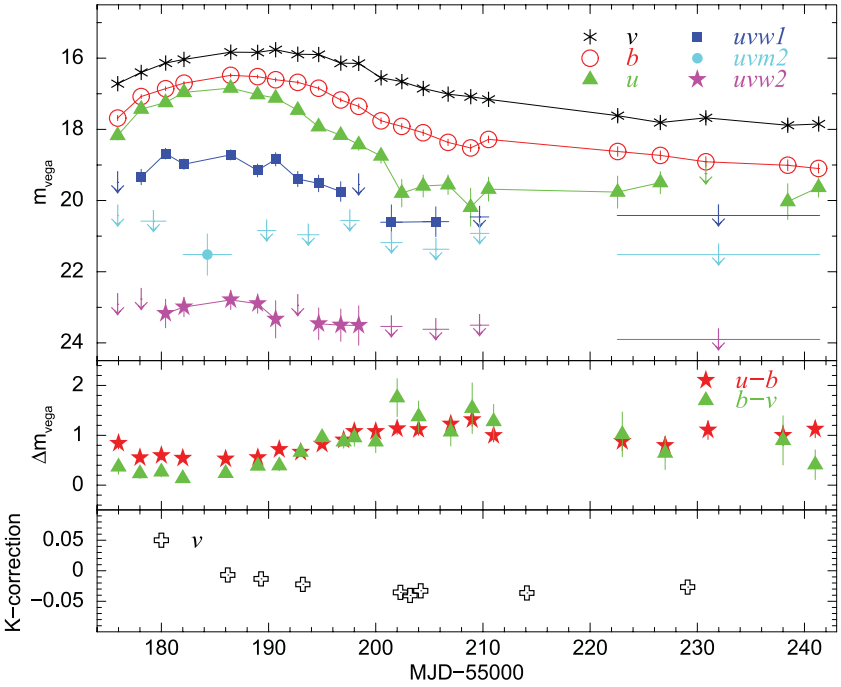

Figure 3. Upper panel: observed UV and optical light curves of SN 2009mg. Middle panel: $(b - v)$ and $(u - b)$ colour curves, corrected for reddening. Lower panel: *K*-correction evolution for the UVOT v filter during the course of UVOT observations.

observed by the *Carnegie Supernova Project* (Stritzinger et al., in preparation). From this method, we estimate an $E(B - V)_{\rm host} = 0.18 \pm 0.04$ mag. This estimate is about a factor of 2 higher than that obtained from the Na I D1 lines.

In what follows, we adopt the weighted mean of our two host colour excess estimates, corresponding to an $E(B - V)_{\rm host} = 0.09 \pm 0.02$ mag. When combined with the Galactic colour excess, we obtain a total colour excess of $E(B - V)_{\rm tot} = 0.14 \pm 0.02$ mag. For an $R_V = 3.1$, this corresponds to an $A_V = 0.43$ mag.

3.2 Photometric evolution

3.2.1 Results

Our broad-band photometric observations of SN 2009mg, which began 3 d after discovery, are plotted in Fig. 3, and extend over a duration of 47 d. There are detections in all bands, but there are fewer detections in the three UV bands compared to the three optical bands. The *uvm*2 band has only one detection from summed observations. The particular brightness of the *uvw*2 band, relative to the *uvm*2 band, is likely to be due to red leak in the former (Brown et al. 2010). Comparing the peak colours of this SN, which are derived below, with the colours of a number of sources (Brown et al. 2010, see their table 12), we find most similarity with a 4000 K blackbody source. This blackbody source required red-leak corrections of ~ -2.25 mag for *uvw*2 and ~ -0.55 mag for *uvw*1.

Observations of the SN light curve began 11 d prior to *B*-band maximum. The rise to maximum is best observed in the *ubv*-band light curves, which show a tendency for the SN to rise faster and peak earlier in the bluest filters. After reaching maximum, the light curves decay at different rates depending on wavelength with the quickest decays observed in the bluest filters. This is consistent with both the observations of most SNe Ib/c and SNe IIb, including SNe 1993J and 2008ax (Schmidt et al. 1993; Lewis et al. 1994; Richmond et al. 1994; Pastorello et al. 2008; Roming et al. 2009a; Taubenberger et al. 2011), and with theoretical predictions (Arnett 1982).

For each filter, the observed peak magnitude ($m_{\rm peak}$) and peak time ($t_{\rm peak}$), listed in Table 1, were determined using an average of 10^5 Monte Carlo simulations of a cubic spline fit to the light curves. The errors for these parameters were taken to be the standard deviation of the simulated distributions. The Monte Carlo simulations were performed on each filter using the first 12 observations; upper limits were not used. Since *uvm*2 has only a single detection, we are not able to use a cubic spline fit to determine $t_{\rm peak}$ and $m_{\rm peak}$, and we therefore do not provide values for these parameters for this filter. To verify our estimates of $t_{\rm peak}$ and $m_{\rm peak}$ for the other filters, we repeated the fitting using a simple polynomial and compared the results to those values derived using the Monte Carlo cubic spline fitting. The values of $m_{\rm peak}$ estimated from the polynomial fits are consistent with cubic spline fits to within 1σ for the optical bandpasses and 2σ for the UV bandpasses. For values of $t_{\rm peak}$, the polynomial fits are consistent with the cubic spline fits, in all filters, to within 1σ. The determination of the peak times of the separate bands (see Table 1) confirms our earlier observation that the bluest filters peak the earliest.

For each filter, we also calculated the absolute peak magnitude ($M_{\rm peak}$) using the observed peak magnitude for each filter and the distance modulus. The resulting values are given in Table 1 and have been corrected for extinction and *K*-correction. To determine the *K*-corrections and extinction corrections, we de-reddened and redshifted to the rest frame a template spectrum from a similar Type IIb SN (SN1993J; Jeffery et al. 1994). The template spectrum of the Type IIb SN, 1993J, was used because the spectral range covers the full bandpass of the UVOT (i.e. 1600–8000 Å). To the spectral template, we applied the $E(B - V)$ values corresponding to the Galactic and host extinction using the Milky Way and Small Magellanic Cloud extinction laws (Cardelli, Clayton & Mathis 1989; Pei

Table 1. Observed UVOT magnitudes and 3σ upper limits, peak times (t_{peak}), peak magnitudes (m_{peak}) and absolute peak magnitudes (M_{peak}). For some of the UV data points, several epochs have been co-added to provide detections and deeper upper limits. The resulting summed exposures are indicated with an * in the time column. Absolute peak magnitudes include extinction and *K*-corrections.

Time	UVOT observed magnitudes					
(MJD-550 00+)	v	b	u	$uvw1$	$uvm2$	$uvw2$
175.92 ± 0.03	16.67 ± 0.07	17.68 ± 0.07	18.17 ± 0.13	>19.49	>20.42	>22.91
178.13 ± 0.04	16.40 ± 0.06	17.08 ± 0.06	17.43 ± 0.08	19.34 ± 0.22	–	>22.77
179.26 ± 1.17*	–	–	–	–	>20.58	–
180.40 ± 0.04	16.14 ± 0.06	16.86 ± 0.06	17.25 ± 0.08	18.68 ± 0.15	–	23.18 ± 0.40
182.11 ± 0.07	16.03 ± 0.05	16.70 ± 0.05	16.96 ± 0.06	18.98 ± 0.15	–	22.99 ± 0.27
184.29 ± 2.25*	–	–	–	–	21.52 ± 0.58	–
186.47 ± 0.07	15.83 ± 0.05	16.48 ± 0.05	16.84 ± 0.07	18.72 ± 0.15	–	22.79 ± 0.27
188.98 ± 0.04	15.76 ± 0.05	16.52 ± 0.05	17.02 ± 0.07	19.15 ± 0.18	–	22.90 ± 0.27
189.82 ± 0.88*	–	–	–	–	>20.84	–
190.66 ± 0.04	15.76 ± 0.06	16.61 ± 0.06	17.12 ± 0.09	18.84 ± 0.19	–	23.34 ± 0.52
192.73 ± 0.03	15.89 ± 0.05	16.68 ± 0.05	17.46 ± 0.08	19.39 ± 0.21	–	>22.94
193.71 ± 1.01*	–	–	–	–	>20.96	–
194.68 ± 0.03	15.90 ± 0.05	16.84 ± 0.06	17.93 ± 0.10	19.52 ± 0.24	–	23.46 ± 0.45
196.74 ± 0.03	16.14 ± 0.06	17.17 ± 0.07	18.16 ± 0.12	19.75 ± 0.28	–	23.50 ± 0.54
197.58 ± 0.87*	–	–	–	–	>20.56	–
198.41 ± 0.04	16.15 ± 0.06	17.35 ± 0.07	18.43 ± 0.16	>19.55	–	23.51 ± 0.56
200.50 ± 0.04	16.55 ± 0.08	17.76 ± 0.08	18.75 ± 0.20	–	–	–
201.47 ± 1.01*	–	–	–	20.61 ± 0.49	>21.18	>23.40
202.44 ± 0.04	16.67 ± 0.07	17.92 ± 0.08	19.79 ± 0.35	–	–	–
204.44 ± 0.03	16.85 ± 0.07	18.10 ± 0.08	19.59 ± 0.30	–	–	–
205.60 ± 1.21*	–	–	–	20.59 ± 0.42	>21.37	>23.62
206.76 ± 0.07	17.01 ± 0.07	18.36 ± 0.09	19.56 ± 0.26	–	–	–
208.86 ± 0.04	17.08 ± 0.08	18.52 ± 0.11	20.19 ± 0.54	–	–	–
209.69 ± 0.87*	–	–	–	>20.46	>20.92	>23.50
210.53 ± 0.04	17.16 ± 0.08	18.28 ± 0.09	19.68 ± 0.34	–	–	–
222.57 ± 0.04	17.62 ± 0.13	18.62 ± 0.13	19.76 ± 0.45	–	–	–
226.56 ± 0.07	17.81 ± 0.13	18.73 ± 0.13	19.50 ± 0.31	–	–	–
230.80 ± 0.11	17.68 ± 0.12	18.91 ± 0.14	>19.24	–	–	–
231.98 ± 9.44*	–	–	–	>20.42	>21.52	>23.90
238.44 ± 0.10	17.88 ± 0.13	19.01 ± 0.16	20.03 ± 0.50	–	–	–
241.32 ± 0.10	17.85 ± 0.11	19.10 ± 0.13	19.63 ± 0.27	–	–	–
m_{peak}	15.75 ± 0.05	16.46 ± 0.04	16.78 ± 0.07	18.56 ± 0.12	–	22.50 ± 0.23
t_{peak}	190.27 ± 1.76	187.40 ± 1.11	184.65 ± 0.94	183.82 ± 3.64	–	187.47 ± 4.32
M_{peak}	−17.68 ± 0.48	−17.10 ± 0.48	−16.95 ± 0.49	−15.30 ± 0.50	–	−11.37 ± 0.53

Table 2. Journal of spectroscopic observations.

Date of observation (UT)	(MJD-55000+)	Epoch[a] (d)	Telescope	Instrument	Spectral range (Å)	Resolution (Å)	Exposure time (s)
21.2 December 2009	186.2	−1.2	CLAY	LDSS3	3900–9300	7	2 × 300
24.3 December 2009	189.3	+1.8	CLAY	LDSS3	3900–9300	7	2 × 300
24.3 December 2009	189.3	+1.8	CLAY	MIKE	3330–9150	0.15	1800
28.2 December 2009	193.2	+5.8	BAADE	IMACS	3976–6362; 6489–10051	9	600
06.3 January 2010	202.3	+14.8	GEMINI-S	GMOS	4201–8429	8	1600
07.2 January 2010	203.2	+15.8	GEMINI-S	GMOS	4199–8426	8	1800
08.2 January 2010	204.2	+16.8	CLAY	LDSS3	3632–9516	7	600
18.1 January 2010	214.1	+26.6	GEMINI-S	GMOS	4201–8428	8	1800
02.1 February 2010	229.1	+41.6	BAADE	IMACS	3976–6357; 6485–10053	9	600
24.0 March 2010	279.0	+91.6	DU PONT	WFCCD	3700–9500	7	900

[a]Days relative to *B*-band maximum.

1992), respectively. The extinction corrections were computed via the subtraction of synthetic magnitudes of an unreddened and reddened template spectrum in the observed frame. The *K*-corrections were computed through the subtraction of synthetic magnitudes from the unreddened template spectrum in the rest and observed frames. The resulting extinction and *K*-correction factors are provided in Table 3. Correcting for extinction and *K*-correction gives a value for the absolute peak v magnitude of SN 2009mg of -17.68 ± 0.48, which is consistent with other SNe IIb (Richardson, Branch & Baron 2006; Drout et al. 2011), including SN 1993J (-17.57 ± 0.24) and SN 2008ax (-17.61 ± 0.43) (Taubenberger et al. 2011).

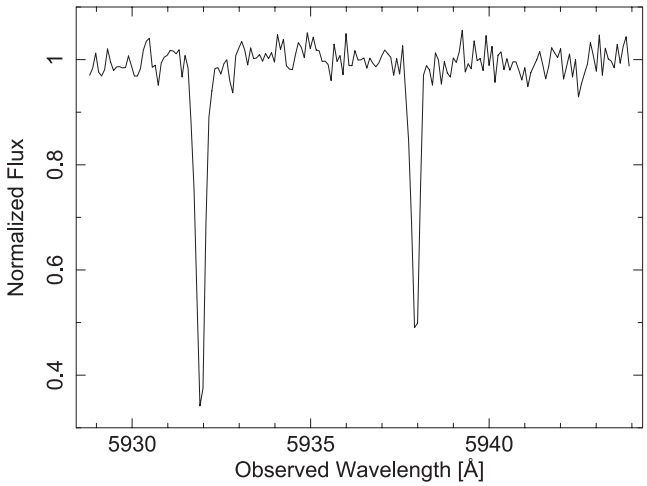

Figure 4. The high-resolution CLAY–MIKE spectrum displaying the Na I D1 λ5931.9 and Na I D2 λ5937.9 lines.

Table 3. Total extinction and *K*-correction factors for the six UVOT bandpasses in magnitudes.

UVOT filter	*v*	*b*	*u*	*uvw1*	*uvm2*	*uvw2*
Extinction	−0.42	−0.55	−0.67	−0.81	−1.09	−0.99
K-correction	0.00	−0.01	−0.05	−0.04	−0.04	−0.03

Plotted in the middle panel of Fig. 3 are the $(u - b)$ and $(b - v)$ colour curves. From the start of observations, with $(u - b) \sim 0.84$ mag and $(b - v) \sim 0.37$ mag, the colour curves are observed to evolve from the red to the blue until the time of photometric maximum, at which point they reach minimum values of 0.52 and 0.14 mag for $(u - b)$ and $(b - v)$, respectively. After photometric maximum, both colour curves evolve towards the red, reaching ∼1 mag, and then cease evolving.

The spectra for SN 2009mg have a spectral range covering the UVOT *v* bandpass; we were therefore able to compute optical *v*-band *K*-corrections. The results are plotted in the lower panel of Fig. 3 at epochs corresponding to when spectroscopic observations were obtained. The evolution of the *K*-correction for the *v* filter tends to follow the $(b - v)$ colour curve evolution. Interestingly, this behaviour mimics what is observed in thermonuclear SNe (Nugent, Kim & Perlmutter 2002).

3.2.2 *Comparison with other SNe IIb*

The brightening to maximum and the subsequent evolution of SN 2009mg's optical light curves follows the classic behaviour of a normal SN IIb. In the top panel of Fig. 5, we compare the *v*-band light curve of SN 2009mg to those of SNe 1993J (Lewis et al. 1994) and 2008ax (Roming et al. 2009a). Note that no extinction corrections have been applied to the photometry and cosmological corrections are ignored since the redshift of each object is low. Here the light curves of SNe 1993J and 2008ax have been scaled to the peak brightness of SN 2009mg. Since the time post-explosion is uncertain for SN 2009mg, the time for this SN has been scaled to the well-constrained explosion date of SN 2008ax. Scaling the time axis of SN 2009mg to that of SN 2008ax allows us to estimate the explosion epoch to be 22 ± 2 d prior to *v*-band maximum, which corresponds to 3 December 2009.

Fig. 5 reveals that the *v*-band light curve of each SN is strikingly similar, particularly from maximum light and onwards. Prior to maximum, the *v*-band light curve of SN 2009mg appears to be slightly broader than the comparison objects. The broader rise for SN 2009mg may be an indication that the ejecta mass of SN 2009mg

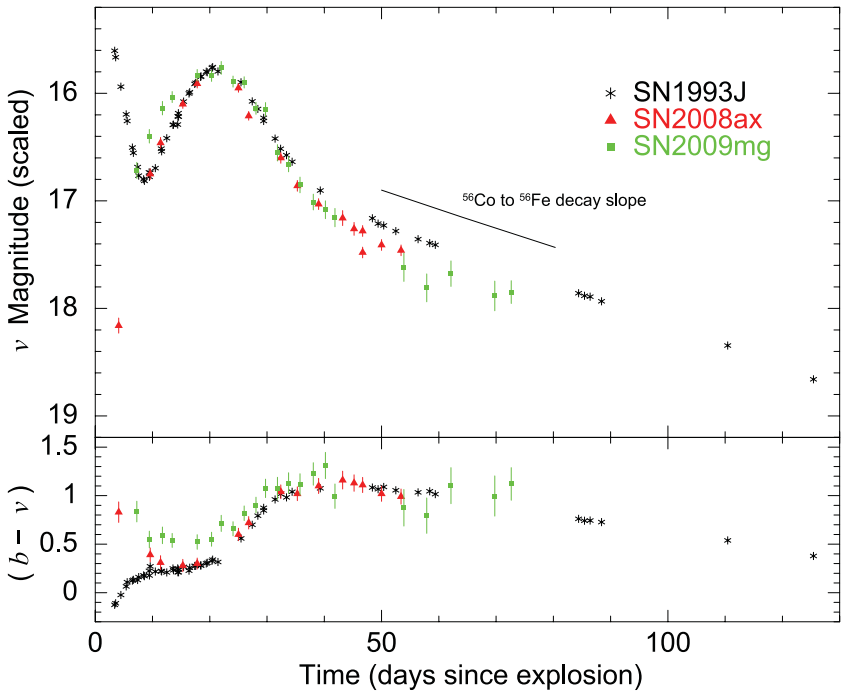

Figure 5. Comparison of the *v*-band light curves of SN 2009mg to those of the prototypical Type IIb SNe 2008ax and 1993J. The top panel shows the *v*-band light curve of SN 2009mg compared with those of SNe 1993J and 2008ax. As the explosion date of SN 2009mg is unknown, the peak time has been shifted to match that of SN 2008ax. The lower panel shows the $(b - v)$ colour evolution for each of these objects, corrected for extinction.

is greater than for SNe 1993J and 2008ax, or the ejecta velocity of SN 2009mg is lower than the comparison objects.

The largest difference between the three objects is observed at the earliest epochs. In SN 1993J, there is an initial drop in luminosity, which is related to a cooling phase that follows shock breakout, while for SN 2008ax, there is a marginal detection of such a decline in the u band (Roming et al. 2009a). No post-shock breakout cooling phase is documented in the v light curve of SN 2009mg, nor at bluer wavelengths (see Fig. 3). This is a strong indication that the observations of SN 2009mg did not commence early enough to catch the initial upturn in luminosity and may also be an indication that the explosion date for SN 2009mg is earlier than the 22 d estimated from comparison with the light curve of SN 2008ax.

From ∼10 d post-explosion, the light curves of all three objects exhibit a similar overall behaviour, a rise to a peak, followed by an exponential decay, which then flattens to a shallower linear decay from ∼40 d. After the peak, they all appear to decay at the same rate. Given the comparison objects are nearly identical to SN 2009mg from maximum light onwards, we attempt to quantify their similarities by measuring the Δm_{15} diagnostic for the b- and v-band light curves. Here Δm_{15} is taken to be the magnitude difference between the peak SN brightness and its brightness measured 15 d post-peak (Phillips 1993).

For the v light curves, we obtain $\Delta m_{15}(v)$ values of 0.948 ± 0.004, 1.19 ± 0.07 and 1.17 ± 0.08 mag for SNe 1993J, 2008ax and 2009mg, respectively. These values of $\Delta m_{15}(v)$ are consistent with, but towards the steeper end of, the range of values determined for a sample of SNe Ib/c V-band light curves (Drout et al. 2011), where the mean $\Delta m_{15}(V)$ for their sample is 0.87 ± 0.25 mag. However, $\Delta m_{15}(v)$ for SN 2008ax is slightly faster than the V-band decline rate found by Taubenberger et al. (2011) and Drout et al. (2011). For the b-band light curve, $\Delta m_{15}(b)$ for the three objects is 1.67 ± 0.01 (SN 1993J), 1.57 ± 0.06 (SN 2008ax) and 1.46 ± 0.09 mag (SN 2009mg), respectively. Note that the value of $\Delta m_{15}(b)$ for SN 2008ax is consistent with the value of $\Delta m_{15}(B)$ obtained by Taubenberger et al. (2011). SN 2009mg declines more slowly in both the v and b bands in comparison to 1993J, while it is more consistent with the evolution of SN 2008ax.

The lower panel of Fig. 5 displays the $(b - v)$ evolution for SNe 1993J, 2008ax and 2009mg. We have applied extinction corrections, with values of $A_v = 0.94$ and $A_b = 1.24$ for SN 2008ax (Roming et al. 2009a), and $A_V = 0.58$ and $A_B = 0.78$ for SN 1993J (Lewis et al. 1994). Although we have not corrected for any systematic offset between the colour curves of each object due to the different photometric systems, these differences are expected to be minimal with $(B - V) \sim (b - v) \sim 0.01$ mag (Poole et al. 2008). From 20 d post-explosion, the $(b - v)$ colour curves exhibit a similar evolution for all three SNe IIb. During the initial 20 d post-explosion, the colour evolution of SN 2009mg is most similar to SN 2008ax. Observations of SN 2009mg commenced at 7 d post-explosion at which $(b - v)$ for SN 2009mg and SN 2008ax is 0.83 and 0.56, respectively. From this point, the colour curves of SNe 2009mg and 2008ax are observed to dip towards the blue, reaching minimum values of $(b - v)$ of ∼0.52 and ∼0.28, respectively. The colour curves then evolve back towards the red, finally levelling off at $(b - v) \sim 1$ before observations ceased. The behaviour of the $(b - v)$ colour curve for SNe 2008ax and 2009mg appear to be a common feature for Type Ib/c and Type IIb SNe (e.g. Roming et al. 2009a; Stritzinger et al. 2009; Drout et al. 2011).

To constrain and compare the late-time temporal behaviour, we computed the decay rate during the shallow decline phase, from 40 d, for the u, b and v light curves of SN 2009mg, and for the V-band light curve of 1993J. The decay rate was computed using a linear least-squares fit. As the observations of SN 2009mg ceased at ∼70 d post-explosion, we fit the linear function to the u, b and v light curves from 40 d post-explosion to the end of observations at ∼70 d. This resulted in decay rates of -0.004 ± 0.011, 0.022 ± 0.004 and 0.025 ± 0.003 mag d^{-1} for the u, b and v light curves, respectively. The decay rate of SN 1993J in the V band during the same period is 0.0213 ± 0.0002 mag d^{-1}, which is consistent with the decay rate of the v filter of SN 2009mg. The v decay rate of SN 2009mg is inconsistent, at 3σ confidence, with the decay rate of ^{56}Co to ^{56}Fe, which is 0.0097 mag d^{-1}. The u-band light curve of SN 2009mg appears to cease decaying at late times, with the decay rate consistent with being constant. Similar behaviour is also observed in the u-band light curves of the Type Ib/IIb SNe 2007Y and 2008aq, which are observed not to decay at late times, but to increase in brightness between ∼20 and ∼90 d post-peak (Stritzinger et al. 2009). The u light curve of SN 2008aq is observed to decrease in brightness again after ∼90 d. The u-band light curve of SN 1993J was also reported to remain almost constant from ∼50 to ∼125 d past maximum (Lewis et al. 1994).

3.3 Optical spectroscopy

The spectroscopic sequence of SN 2009mg, shown in Fig. 6, reveals the typical evolution of an SN IIb. At early phases, Hα and absorption features associated with Fe II and Ca II dominate the spectrum. In addition, during the earliest observed epochs features attributed to He I and Na I are also discernible and, over time, grow in strength.

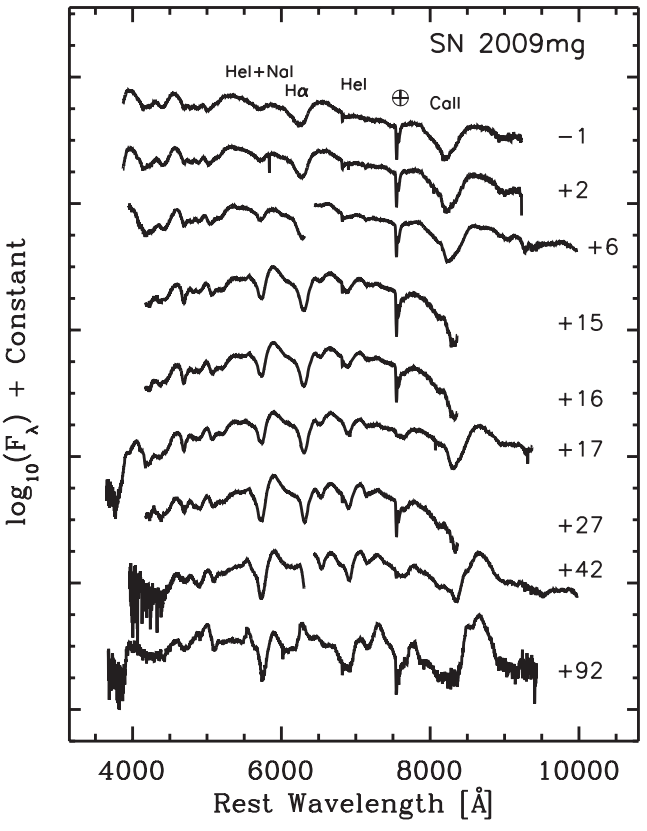

Figure 6. Spectroscopic sequence of SN 2009mg ranging from −1 to +92 d relative to B-band maximum. Each spectrum has been corrected to the rest frame of the host galaxy adopting the redshift $z = 0.0076$, and for presentation purposes shifted in flux by an arbitrary constant.

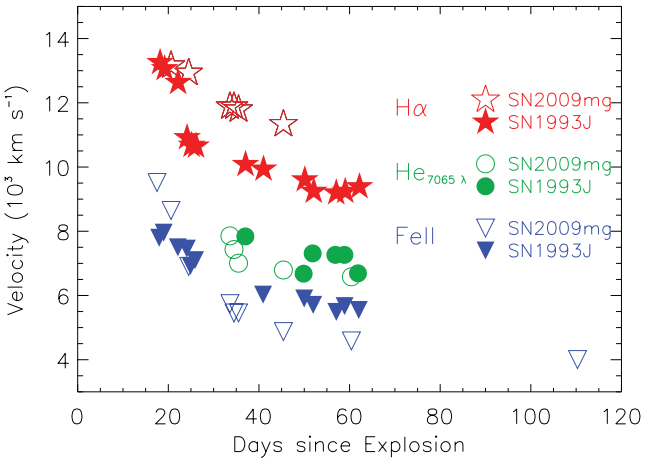

Figure 7. Time evolution of line velocities for Hα, He I λ7065 and Fe II λ5169. For comparison, the evolution of same line velocities for SN 1993J is plotted (Pastorello et al. 2008).

As is common for SNe IIb, the strength of the He I lines compared to Hα increased as the SN evolved. In the case of SN 2009mg, the relative strength does not appear to grow as quickly as in SN 2008ax. For SN 2008ax, Hα and He I λ5876 were of comparable strength ∼30 d after the explosion, while the Hα absorption was negligible by +56 d post-explosion (Pastorello et al. 2008). For SN 2009mg, assuming an explosion date of 3 December 2009, the signal-to-noise ratio of these two features is comparable in strength by day 45 post-explosion. Our series of spectra do not allow us to place confirm constraints on the epoch in which Hα completely disappears; however, Hα is still strong 60 d after the explosion, and is absent in our next spectrum taken on 110 d post-explosion.

In Fig. 7, we plot the time evolution of the blueshifts of the absorption features due to Hα, Fe II λ5169 and He I λ7065. Included in this figure is also the time evolution of these lines determined from the spectroscopic sequence of SN 1993J (Pastorello et al. 2008). These measurements were determined from the minima of the P Cygni features. The evolution of the He I line is similar in both objects, while for Hα, the velocity is similar at the start of the observations, but unlike SN 1993J, the strength of this feature in SN 2009mg does not drop steeply after day 25, but remains consistently higher. The Fe II line velocity of SN 1993J is found to be higher at the start of observations in comparison to SN 2009mg, but declines at a faster rate. It is interesting to compare Fig. 7 with the equivalent figure for SN 2008ax in Pastorello et al. (2008, see their fig. 6). The evolution of the line velocities of Hα, He I λ7065 and Fe II λ5169 for both SNe 2008ax and SN 2009mg behaves very similarly, although the Hα line in SN 2008ax remains at a slightly higher velocity at late times compared to SN 2009mg and Fe II λ5169 drops off at slightly a faster rate for SN 2008ax. This may suggest that the H envelope mass and the blastwave evolution are similar for the two SNe.

3.4 X-ray observations and mass-loss rate

Analysis of the X-ray observations shows no significant detection for SN 2009mg. Using a standard 10-pixel radius (24.5 arcsec) source region and extracting the background from a local, source-free region to account for sky background and for diffuse emission from the host galaxy, the 3σ upper limit to the XRT net count rate is 5.3×10^{-4} counts s^{-1}. This corresponds to an unabsorbed (0.2–10 keV band) X-ray flux of $<2.5 \times 10^{-14}$ erg cm^{-1} s^{-1}, and a luminosity of $<5.0 \times 10^{39}$ erg s^{-1} for an adopted thermal plasma spectrum with a temperature of kT = 10 keV, a Galactic foreground column density of $N_H = 3.5 \times 10^{20}$ cm^{-2} (Dickey & Lockman 1990) and a distance of 33 Mpc. The upper limit derived for the luminosity is consistent with values determined for other stripped core-collapse SNe including SN 2008ax (Immler et al. 2006, 2007; Roming et al. 2009a).

In core-collapse SNe, the likely cause of X-ray emission is the interaction of the SN blastwave with circumstellar material (Chevalier 1982; Immler, Aschenbach & Wang 2001; Immler et al. 2007). We use the X-ray non-detection to place an upper limit on the mass-loss rate of the progenitor. Following the methodology described in Immler et al. (2007), we derive a mass-loss rate of $<1.5 \times 10^{-5}$ M$_\odot$ yr^{-1}(v_w/10 km s^{-1}), assuming the speed of the blastwave as $v_s = 10\,000$ km s^{-1} and scaled for a stellar wind speed of $v_w = 10$ km s^{-1}. The velocity of the Fe II λ5169 feature is representative of the velocity of the photosphere (Dessart & Hillier 2005). Therefore, we are able to assume a value of 10 000 km s^{-1} for the blastwave velocity, since the peak velocity of Fe II λ5169 feature is approximately 10 000 km s^{-1} at maximum light. The blastwave velocity is proportional to the mass-loss rate and so assuming a blastwave velocity of 10 000 km s^{-1}, rather than using an average value from across the duration of the XRT observations, gives us a conservative upper limit to the mass-loss rate. The resulting 3σ upper limit lies within the range of the mass-loss rate determined for SN 1993J (10^{-5}–10^{-4}; Immler et al. 2007), and is also consistent with SN 2008ax ($(9 \pm 3) \times 10^{-6}$; Roming et al. 2009a) and Type IIP SNe (10^{-6}–10^{-5}; Chevalier, Fransson & Nymark 2006; Immler et al. 2007), which have also been shown to have low mass-loss rates.

4 DISCUSSION

As we have shown in the previous section, the observation properties of SN 2009mg closely resemble those of other normal SNe IIb. We now endeavour to place limits on the explosion properties of this object.

Using the method described by Richardson et al. (2006), we proceed to model the v-band light curve of SN 2009mg to provide reasonable estimates on the kinetic energy (E_k), ejected mass (M_{ej}) and ejected nickel mass (M_{Ni}). This simple analytic method uses the model of Arnett (1982) to describe the peak of the light curve while the linear tail is best represented by the model of Jeffery (1999). To constrain these three parameters, a Monte Carlo simulation of the v-band light curve of SN 2009mg was computed with 10^6 realizations. This analysis is best performed using the UVOIR light curve, but there are no IR observations of this SN to our knowledge. Since the v-band light curve is a reasonable proxy for the bolometric light curve, we use this as a substitute for the UVOIR light curve and apply a Bolometric correction of −1.48 mag, as described in Richardson et al. (2006). In this simulation, the routine switches from the Arnett model to the Jeffery model at day 31 post-explosion. The best χ^2 fit (χ^2/DOF = 1.1) results in $E_k = 0.15^{+0.02}_{-0.13} \times 10^{51}$ erg, $M_{ej} = 0.56^{+0.10}_{-0.26}$ M$_\odot$ and $M_{Ni} = 0.10 \pm 0.01$ M$_\odot$. The best-fitting model is shown in Fig. 8. The resultant parameters are similar to, but lower than, the values calculated by Richardson et al. (2006) for the Type IIb SNe 1996cb and 1993J. Since the Jeffery model assumes that the ^{56}Ni has decayed and the ejecta is optically thin, it should ideally be fit to data between ∼100 and ∼150 d. We therefore verified our result by repeating the simulation, fixing the time at which the simulation transfers from the Arnett to the Jeffery model to be 50 d post-explosion. The resulting values for E_k, M_{ej} and M_{Ni}

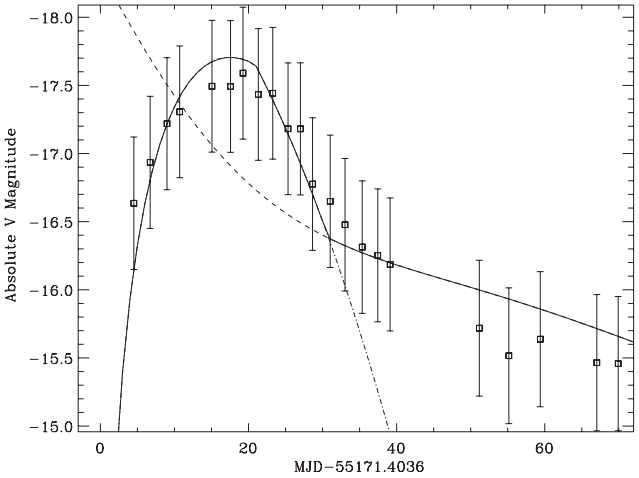

Figure 8. The best fit to the v-band light curve following the methodology of Richardson et al. (2006). The dot–dashed line shows the fit using the Arnett model, while the dashed line shows the fit of the Jeffery model. The overall combined best-fitting model is given by the solid line.

are consistent with the values determined with the transfer at 31 d post-explosion.

The favoured progenitors, of SNe IIb, are massive stars in binary systems (Smith et al. 2011; Claeys et al. 2011, see references within). Models of stripped helium stars in binary systems, are provided by Shigeyama et al. (1990) and Podsiadlowski et al. (1993). Shigeyama et al. (1990) conclude that smaller helium stars undergo more extensive mixing and eject smaller masses than larger helium stars and so form light curves with steeper tails. This is because the ejecta is more transparent when the ejecta mass is small and mixed (Shigeyama et al. 1990; Iwamoto et al. 1997), and thus allows more γ-rays to escape before they can be thermalized. When γ-rays are fully trapped the light curves decay slowly at a rate consistent with the decay rate of ^{56}Co. Therefore, one indication of the degree of mixing in the progenitor is the decay rate of the tail of the light curve. The decay rate of the tail of SN 2009mg in the v band is 0.025 ± 0.003 mag d^{-1}, which is steeper, at 3σ confidence, than the decay rate of ^{56}Co to ^{56}Fe, which decays at a rate of 0.0097 mag d^{-1} (see Fig. 5). This suggests that there is leakage of γ-rays and hence some degree of mixing of the progenitor (Shigeyama et al. 1990). This would indicate that the progenitor is likely to be on the small side of the mass distribution. This is consistent with the light-curve modelling, which suggests values of $E_{\rm k}$, $M_{\rm ej}$ and $M_{\rm Ni}$ similar to, but lower than, those of 1993J and 1996cb.

5 CONCLUSIONS

SN 2009mg appears to be a normal SN IIb and exhibits properties similar to other normal, well-observed SNe IIb. Modelling the v-band light curve, we find best-fitting parameters for kinetic energy ($E_{\rm k}$) of $0.15^{+0.02}_{-0.13} \times 10^{51}$ erg, an ejecta mass ($M_{\rm ej}$) of $0.56^{+0.10}_{-0.26}$ M$_\odot$ and a nickel mass ($M_{\rm Ni}$) of 0.10 ± 0.01 M$_\odot$.

The decline rate of the light-curve tail starting from 40 d past B-band maximum is inconsistent, at 3σ confidence, with the decline rate of ^{56}Co. This indicates that there is leakage of γ-rays out of the ejecta and suggests that the progenitor star was on the lower end of the stellar mass distribution.

ACKNOWLEDGMENTS

We thank the referee for their useful comments. We also thank N. Morrell for performing spectroscopic observations. This research has made use of data obtained from the High Energy Astrophysics Science Archive Research Center (HEASARC) and the Leicester Database and Archive Service (LEDAS), provided by NASA's Goddard Space Flight Center and the Department of Physics and Astronomy, Leicester University, UK, respectively. SRO, AAB and NPMK acknowledge the support of the UK Space Agency. JLP acknowledges support from NASA through Hubble Fellowship Grant HF-51261.01-A awarded by STScI, which is operated by AURA, Inc. for NASA, under contract NAS 5-2655. MH acknowledges support by CONICYT through Centro de Astrofisica FONDAP 15010003, Centro BASAL CATA (PFB 06) and by Iniciativa Cientifica Milenio through the Millennium Center for Supernova Science (P10-064-F).

REFERENCES

Arcavi I. et al., 2011, ApJ, 742, L18
Arnett W. D., 1982, ApJ, 253, 785
Barbon R., Buondí V., Cappellaro E., Turatto M., 1999, A&AS, 139, 531
Bietenholz M. F., Brunthaler A., Soderberg A. M., Krauss M., Bartel N., Chomiuk L., Rupen M. P., 2012, ApJ, 751, 125
Breeveld A. A., Landsman W., Holland S. T., Roming P., Kuin N. P. M., Page M. J., 2011, in McEnery J. E., Racusin J. L., Gehrels N., eds, Proc. AIP Conf. Ser. Vol. 1358, Gamma Ray Bursts 2010. Am. Inst. Phys., New York, p. 373
Brown P. J. et al., 2009, AJ, 137, 4517
Brown P. J. et al., 2010, ApJ, 721, 1608
Burrows D. N. et al., 2005, Space Sci. Rev., 120, 165
Cardelli J. A., Clayton G. C., Mathis J. S., 1989, ApJ, 345, 245
Chevalier R. A., 1982, ApJ, 259, 302
Chevalier R. A., Soderberg A. M., 2010, ApJ, 711, L40
Chevalier R. A., Fransson C., Nymark T. K., 2006, ApJ, 641, 1029
Chornock R. et al., 2011, ApJ, 739, 41
Claeys J. S. W., de Mink S. E., Pols O. R., Eldridge J. J., Baes M., 2011, A&A, 528, A131
Dessart L., Hillier D. J., 2005, A&A, 439, 671
Dickey J. M., Lockman F. J., 1990, ARA&A, 28, 215
Drout M. R. et al., 2011, ApJ, 741, 97
Filippenko A. V., 1988, AJ, 96, 1941
Filippenko A. V., 1997, ARA&A, 35, 309
Filippenko A. V., Matheson T., Ho L. C., 1993, ApJ, 415, L103
Gehrels N. et al., 2004, ApJ, 611, 1005
Green D. W. E., 2008, Cent. Bureau Electron. Telegrams, 1227, 3
Hamuy M. et al., 2009, ApJ, 703, 1612
Immler S., Aschenbach B., Wang Q. D., 2001, ApJ, 561, L107
Immler S. et al., 2006, ApJ, 648, L119
Immler S. et al., 2007, ApJ, 664, 435
Iwamoto K., Young T. R., Nakasato N., Shigeyama T., Nomoto K., Hachisu I., Saio H., 1997, ApJ, 477, 865
Jeffery D. J., 1999, preprint (arXiv:e-prints)
Jeffery D. J. et al., 1994, ApJ, 421, L27
Koribalski B. S. et al., 2004, AJ, 128, 16
Lewis J. R. et al., 1994, MNRAS, 266, L27
Maund J. R., Smartt S. J., Kudritzki R. P., Podsiadlowski P., Gilmore G. F., 2004, Nat, 427, 129
Maund J. R. et al., 2011, ApJ, 739, L37
Monard L. A. G., 2009, Cent. Bureau Electron. Telegrams, 2071, 1
Munari U., Zwitter T., 1997, A&A, 318, 269
Nomoto K., Suzuki T., Shigeyama T., Kumagai S., Yamaoka H., Saio H., 1993, Nat, 364, 507
Nugent P., Kim A., Perlmutter S., 2002, PASP, 114, 803
Pastorello A. et al., 2008, MNRAS, 389, 955
Pei Y. C., 1992, ApJ, 395, 130

Phillips M. M., 1993, ApJ, 413, L105
Podsiadlowski P., Hsu J. J. L., Joss P. C., Ross R. R., 1993, Nat, 364, 509
Poole T. S. et al., 2008, MNRAS, 383, 627
Prieto J., 2009, Cent. Bureau Electron. Telegrams, 2087, 1
Qiu Y., Li W., Qiao Q., Hu J., 1999, AJ, 117, 736
Richardson D., Branch D., Baron E., 2006, AJ, 131, 2233
Richmond M. W., Treffers R. R., Filippenko A. V., Paik Y., Leibundgut B., Schulman E., Cox C. V., 1994, AJ, 107, 1022
Roming P. W. A. et al., 2000, in Flanagan K. A., Siegmund O. H. W., eds, Proc. SPIE Vol. 4140, X-Ray and gamma-Ray Instrumentation for Astronomy XI. SPIE, Bellingham, p. 76
Roming P. W. A. et al., 2004, in Flanagan K. A., Siegmund O. H. W., eds, Proc. SPIE Vol. 5165, X-Ray and gamma-Ray Instrumentation for Astronomy. SPIE, Bellingham, p. 262
Roming P. W. A. et al., 2005, Space Sci. Rev., 120, 95
Roming P. W. A. et al., 2009a, ApJ, 704, L118
Roming P. W. A., Prieto J., Milne P. A., 2009b, Cent. Bureau Electron. Telegrams, 2093, 1
Schlegel D. J., Finkbeiner D. P., Davis M., 1998, ApJ, 500, 525
Schmidt B. P. et al., 1993, Nat, 364, 600
Shigeyama T., Nomoto K., Tsujimoto T., Hashimoto M.-A., 1990, ApJ, 361, L23
Smith N., Li W., Filippenko A. V., Chornock R., 2011, MNRAS, 412, 1522
Soderberg A. M. et al., 2012, ApJ, 752, 78
Stritzinger M., 2010, Cent. Bureau Electron. Telegrams, 2158, 1
Stritzinger M. et al., 2009, ApJ, 696, 713
Swartz D. A., Clocchiatti A., Benjamin R., Lester D. F., Wheeler J. C., 1993, Nat, 365, 232
Taubenberger S. et al., 2011, MNRAS, 413, 2140
Van Dyk S. D. et al., 2011, ApJ, 741, L28
Wheeler J. C., Levreault R., 1985, ApJ, 294, L17
Woosley S. E., Langer N., Weaver T. A., 1993, ApJ, 411, 823
Woosley S. E., Langer N., Weaver T. A., 1995, ApJ, 448, 315

This paper has been typeset from a TEX/LATEX file prepared by the author.